2b) shows that natural cleavage planes (corresponding to van der Waals contacts between layers of molecules) are approximately normal to the c direction.
(7) (a) D. H. Templeton and L. K. Templeton, Abstracts, American Crystallographic Association Meeting, Storrs, Conn., 1973, No. E10; (b) N. W. Alcock in "Crystallographic Computing", F. R. Ahmed, Ed., Munksgaard, Copenhagen, 1970, p 271; (c) J. de Meulenaer and H. Tompa, *Acta Crystallogr.*, **19**, 1014 (1965).
(8) The crystal was assumed to be bounded by seven planes with Miller indices (100), (100), (001), (001), (011), (01$\bar{1}$), and ($\bar{1}$10).
(9) W. R. Busing, K. O. Martin, and H. A. Levy, ORFLS, Oak Ridge National Laboratory Report ORNL-TM-305, 1962.
(10) P. J. Becker and P. Coppens, *Acta Crystallogr., Sect. A*, **30**, 129 (1974). The extinction model chosen was type I with a Lorentzian mosaic distribution.
(11) C. G. Shull, private communication, 1972.
(12) Esd's were obtained from the variance–covariance matrix prepared in a final cycle of refinement, where positional parameters for all atoms were varied, and thermal parameters were held fixed. A local modification of program ORFFE was used for these calculations: W. R. Busing, K. O. Martin, and H. A. Levy, Oak Ridge National Laboratory Report ORNL-TM-306, 1964.
(13) The Cp rings are numbered corresponding to the Ni atoms to which they are bonded.
(14) "Tables of Interatomic Distances and Configuration in Molecules and Ions", Supplement 1956–1959, *Chem. Soc., Spec. Publ.*, **No. 18**, S 8s (1965).
(15) O. S. Mills and B. W. Shaw, *J. Organomet. Chem.*, **11**, 595 (1968).
(16) A. A. Hock and O. S. Mills in "Advances in the Chemistry of Coordination Compounds", S. Kirschner, Ed., Macmillan, New York, 1961, p 640.
(17) (a) O. Jarchow, H. Schultz, and R. Nast, *Angew. Chem., Int. Ed. Engl.*, **9**, 71 (1970); *Angew. Chem.*, **82**, 43 (1970); (b) O. Jarchow, *Z. Kristallogr., Kristallgeom., Kristallphys., Kristallchem.*, **136**, 122 (1972).
(18) O. Jarchow, *Z. Anorg. Allg. Chem.*, **383**, 40 (1971).
(19) R. Hoffmann, B. E. R. Schilling, R. Bau, H. D. Kaesz, and D. M. P. Mingos, *J. Am. Chem. Soc.*, **100**, 6088 (1978).
(20) For purposes of comparison, the mean Co–Co distance in the 60-electron cluster $H_4Co_4Cp_4$ is 2.467 (5) Å (ref 4b), or 0.039 Å shorter than the value of 2.506 Å found in cobalt metal (ref 14, S 5s).
(21) R. G. Teller, R. D. Wilson, R. K. McMullan, T. F. Koetzle, and R. Bau, *J. Am. Chem. Soc.*, **100**, 3071 (1978).
(22) A. Haaland, *Top. Curr. Chem.*, **53**, 1 (1975).
(23) F. Takusagawa and T. F. Koetzle, *Acta Crystallogr.*, in press.
(24) F. Takusagawa and T. F. Koetzle, to be published.
(25) J. L. Petersen, L. F. Dahl, and J. M. Williams, *J. Am. Chem. Soc.*, **96**, 6610 (1974).
(26) R. D. Wilson, T. F. Koetzle, D. W. Hart, Å. Kvick, D. L. Tipton, and R. Bau, *J. Am. Chem. Soc.*, **99**, 1775 (1977).
(27) R. Stockmeyer, H. M. Conrad, A. Renouprez, and P. Fouilloux, *Surf. Sci.*, **49**, 549 (1975).
(28) (a) D. J. M. Fassaert, H. Verbeek, and A. van der Avoird, *Surf. Sci.*, **29**, 501 (1972); (b) D. J. M. Fassaert and A. van der Avoird, *ibid.*, **55**, 291 (1976); (c) *ibid.*, **55**, 313 (1976).
(29) A. J. Renouprez, P. Fouilloux, G. Coudurier, D. Tocchetti, and R. Stockmeyer, *J. Chem. Soc., Faraday Trans. 1*, **73**, 1 (1977).
(30) R. D. Kelley, J. J. Rush, and T. E. Madey, submitted for publication.
(31) For a complete listing of stretching frequencies associated with bridging and triply bridging hydride ligands in covalent metal hydride complexes, see Table II in C. B. Cooper, III, D. F. Shriver, and S. Onaka, *Adv. Chem. Ser.*, **No. 167**, 232 (1978).
(32) G. Doyen and G. Ertl, *J. Chem. Phys.*, **68**, 5417 (1978).
(33) G. Blyholder, *J. Chem. Phys.*, **62**, 3193 (1975).
(34) (a) M. A. van Hove, G. Ertl, K. Christmann, R. J. Behm, and W. H. Weinberg, *Solid State Commun.*, **28**, 373 (1978); (b) K. Christmann, R. J. Behm, G. Ertl, M. A. van Hove, and W. H. Weinberg, *J. Chem. Phys.*, **70**, 4168 (1979).
(35) However, in the LEED studies, ordered adsorbed layers were formed only below room temperature, and the potential energy barrier to diffusion of hydrogen on the surface is evidently quite low.
(36) T. H. Upton and W. A. Goddard, III, *Phys. Rev. Lett.*, **42**, 472 (1979).
(37) (a) G. Herzberg, "Spectra of Diatomic Molecules", Van Nostrand-Reinhold, Princeton, N.J., 1950; (b) A. Heimer, *Z. Phys.*, **105**, 56 (1937).
(38) For purposes of comparison, neutron diffraction measurements have indicated that H atoms occupy octahedral sites in the fcc lattice in nickel hydride ($NiH_{0.6}$), with a Ni–H distance of 1.86 Å [E. O. Wollan, J. W. Cable, and W. C. Koehler, *J. Phys. Chem. Solids*, **24**, 1141 (1963)]. This value is very close to the Co–H distance of 1.82 (1) Å found recently for the six-coordinated H atom in the covalent cluster $[HCo_6(CO)_{15}]^-$ [D. W. Hart, R. G. Teller, C. Y. Wei, R. Bau, G. Longoni, S. Campanella, P. Chini, and T. F. Koetzle, *Angew. Chem., Int. Ed. Engl.*, **18**, 80 (1979); *Angew. Chem.*, **91**, 86 (1979)].
(39) For an up-to-date tabulation of metal–hydrogen bonds analyzed by single-crystal neutron diffraction techniques, see R. Bau, R. G. Teller, S. W. Kirtley, and T. F. Koetzle, *Acc. Chem. Res.*, **12**, 176 (1979).
(40) L. Hedberg and K. Hedberg, *J. Chem. Phys.*, **53**, 1228 (1970).
(41) H. Vahrenkamp and L. F. Dahl, *Angew. Chem., Int. Ed. Engl.*, **8**, 144 (1969); *Angew. Chem.*, **81**, 152 (1969).
(42) H. Vahrenkamp, V. A. Uchtman, and L. F. Dahl, *J. Am. Chem. Soc.*, **90**, 3272 (1968).
(43) C. K. Johnson, ORTEP-II, Oak Ridge National Laboratory Report ORNL-5138, 1976.

Analysis of the Oscillations in "Beating Mercury Heart" Systems

Joel Keizer,* Peter A. Rock,* and Shu-Wai Lin[1]

Contribution from the Chemistry Department, University of California, Davis, California 95616. *Received February 12, 1979*

Abstract: A column of mercury whose top surface is covered with aqueous acid or base undergoes periodic changes in height when the surface is brought into contact with a corroding metal electrode. The voltage between the mercury and the corroding electrode also undergoes periodic changes which we have followed on an oscilloscope. We present here a thorough analysis of a mechanism for these oscillations which is based on the effect of voltage and adsorption on the surface tension of mercury. Oscillations in sulfuric acid solutions of strong oxidants, such as $Cr_2O_7^{2-}$(aq), apparently are associated with a film of Hg_2SO_4 on the mercury. The reduction of this film by the corroding electrode—or, in the absence of strong oxidants, the reduction of electron acceptors such as O_2(aq)—modifies the surface tension of mercury. For an appropriate placement of the corroding electrode and the mercury, the altered surface tension switches the direction in which the surface moves. This effect breaks electrical contact between the mercury and the corroding electrode, so that the voltage of the mercury is free to rise as the oxidation or reduction process proceeds. The increasing voltage, in turn, modifies the surface tension in such a manner as to bring the mercury and electrode back into contact, completing the oscillation. We support this mechanism with quantitative measurements of the oscillations under a variety of conditions. Finally we show that the limit-cycle oscillations which occur in a simple mathematical model of this mechanism are in close correspondence to the observed oscillations.

I. Introduction

Oscillations in electrochemical systems have been known for many years,[2,3] although they have often been treated as curiosities of little consequence. Recently, however, it has been recognized that oscillations are among the novel kinds of phenomena that can occur in systems which are far from equilibrium.[4-6] For these sort of systems it is apparent that the kinetic point of view is more fundamental than the thermodynamic. In fact, the kinetic point of view is more fundamental than the thermodynamic, quite generally, if one takes cognizance of the molecular mechanisms which underlie the kinetics.[7] In chemical investigations this molecular perspective is mandatory, and we adopt it here.

It is our purpose in this communication to describe work

0002-7863/79/1501-5637$01.00/0

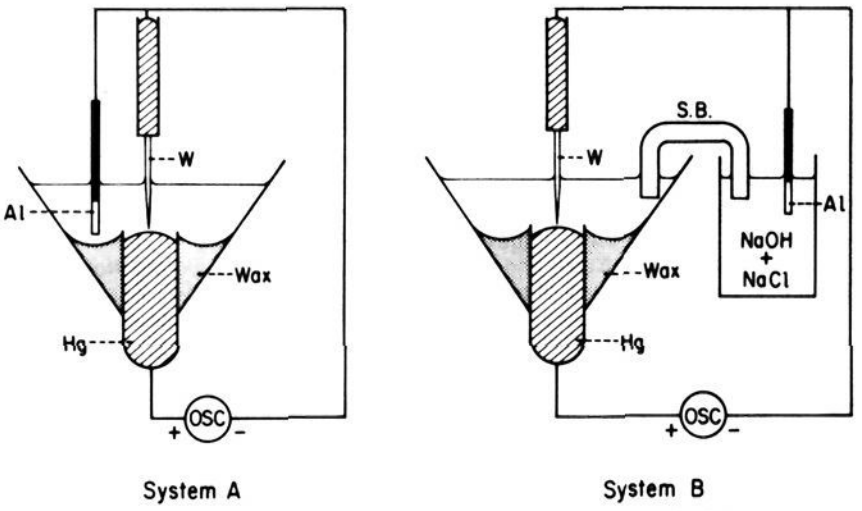

Figure 1. The apparatus in which oscillations are studied. In this geometry the mercury meniscus is convex and the center of the meniscus is initially set even with the top of the tube. In A, the corroding electrode (Al) is in the same vessel as the mercury. In B, the corroding metal is located in a separate container connected to the solution above the mercury by a 1.0 M NaCl salt bridge (S.B.). The polarity of the oscilloscope (OSC) is as indicated. For the iron wire/acidic dichromate/mercury system the setup is the same except that Fe replaces Al and the tungsten tip is placed near the perimeter of the mercury surface.

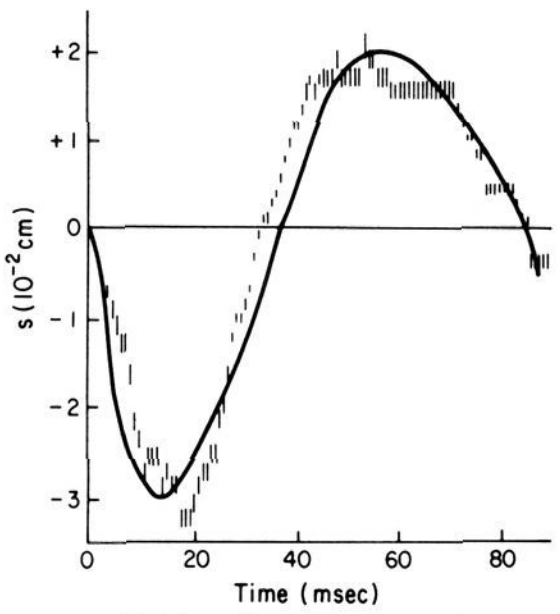

Figure 2. Separation of W-tip and the mercury surface as a function of time for the Al(W)|OH^-(aq),O_2(aq)|Hg(l) oscillator. The experimental data is designated by vertical error bars. Analysis of the film data was carried out with the aid of a Photo Optical Data Analyzer (L.W. Van Nuys, Model 224A). The solid line comes from the limit cycle oscillation for model I with $\gamma_0 = 391$, $Y = 280$, $D = 45$, $i_0 = 1.35 \times 10^{-3}$, $L = 0.17$, and other parameters listed in ref 27.

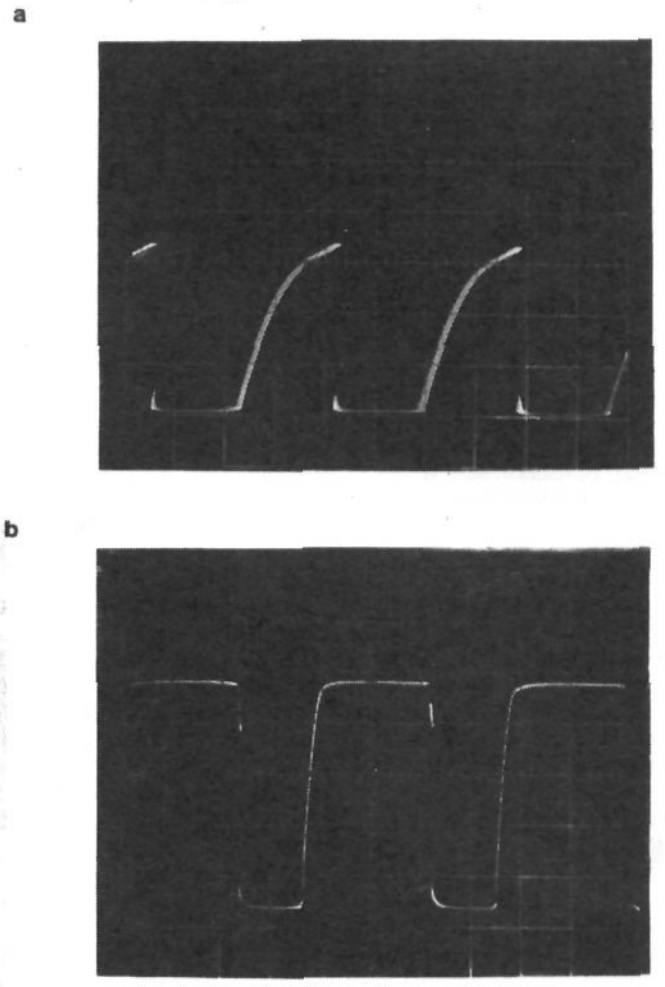

Figure 3. Typical oscilloscope traces of spontaneous oscillations for the oscillators: (a) Al(W)|NaCl(aq),NaOH(aq),O_2(aq)|Hg(l) and (b) Fe(W)|$K_2Cr_2O_7$(aq),H_2SO_4(aq)|Hg(l). The vertical axis is the Hg to M(W) voltage difference, v, which is always positive (one large division is 50 mV in (a) and 200 mV in (b)); the horizontal axis is time (one large division is 20 ms). On the portion of the curve where the voltage is constant, the *flat line*, $v = 0.1$ mV. The *period* is the time between two voltage peaks, and the duration of the rising voltage is the *rise time*. The difference between the highest voltage during a period and the flat line is the *peak height*.

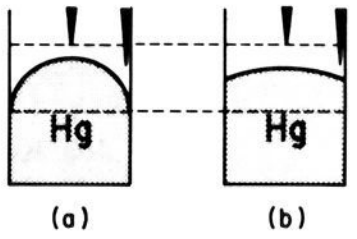

Figure 4. (a) represents the geometry of the mercury surface at a low surface tension and (b) represents a high surface tension. At higher surface tension the center-to-tip separation is larger and the side-to-tip separation is smaller.

elucidating the molecular mechanism of certain electrochemical–mechanical oscillators. The original oscillator of this sort was observed by Kühne and reported by Lippmann[8,9] in connection with his work on electrocapillarity. Previously we have described a simplified version of these oscillations[10] which occur in the geometry of Figure 1. Mercury in a glass tube is covered at the top surface by an acidic or basic solution. In base a piece of corroding aluminum is connected to a sharpened tungsten tip which is brought into contact with the mercury meniscus. This results in a rapid motion of mercury which we have measured quantitatively using high-speed motion-picture photography. This oscillation is shown in Figure 2. The voltage between the mercury and the tungsten, $v = \phi_{Hg} - \phi_{Al(W)}$, also varies periodically in time as shown in Figure 3a.

The oscillations occur as soon as the tungsten tip is placed into position, and we have observed no induction period for the oscillations. When acidic solutions are used, an iron electrode is substituted for the aluminum electrode; this gives rise to the voltage oscillations in Figure 3b. The duration of the flat portion at the bottom of the voltage–time curve is called the flat-line time, the maximum voltage difference is called the peak height, and the time between the end of the flat-line and the maximum is the rise time. These features are characteristic of the oscillations. Much of our mechanistic work is based on quantitative measurement of the effect of chemical and physical changes on the voltage curves.

Whether or not oscillations are actually obtained depends on the positioning of the electrode tip with respect to the mercury. We have observed two situations: oscillations that can be triggered near the perimeter of the mercury surface only, and those that can be triggered only from near the center. There is a significant geometric difference between these two situations. As shown in Figure 4, the center-tip distance *increases* as the surface flattens, whereas the perimeter-tip distance *decreases*. A flatter surface corresponds to a higher surface tension, so that an increase in surface tension affects the center-to-tip and perimeter-to-tip distance in opposite ways. This geometric difference in the oscillations is related to film formation on the mercury surface and is explored further in section III.

On the flat-line portion of the voltage traces, the voltage difference between the mercury and the tip is about 0.1 mV. Although it is difficult to verify by eye that the tip and mercury actually come into physical contact, we have demonstrated this clearly using rapid-motion-picture photography. This also has allowed us to establish the phase relationship between the voltage and separation curves. The flat-line portion of the voltage curve corresponds to the negative separations in Figure 2. When the separation becomes zero, contact is broken, and the voltage begins to rise as indicated in Figures 3a and 3b. The separation achieves its maximum value before the voltage, and then decreases until contact is again restored. This is the short circuit that causes the sudden decrease in the voltage[10] and which is complete within 10^{-6}-10^{-7} s.

II. Nature of the Chemistry

The significant chemical processes in the mercury heart oscillations occur at the mercury and corroding metal surfaces. The electron-transfer steps depend on the voltage of the surfaces and the concentrations of reducing or oxidizing species in solutions.[11,12] Furthermore, the shape of the mercury surface is dependent on the voltage of the surface and the nature and amount of adsorbed species on the surface. This is the equilibrium electrocapillary effect[13] and is caused by the dependence of the surface tension on these variables.

The driving force for the oscillations is the corrosion of either iron in aqueous acid or aluminum in aqueous base.[10] While the detailed mechanisms of both these corrosion processes are not completely understood, the net processes are evidently[11,12]

$$Fe + 2H^+(aq) = Fe^{2+}(aq) + H_2(g) \quad (1)$$

and

$$2Al + 2OH^-(aq) + 6H_2O = 2Al(OH)_4^- + 3H_2(g) \quad (2)$$

In 0.5 M H_2SO_4(aq) we have measured the corrosion voltage of iron as 0.90 V with respect to the mercury electrode. In 0.02 M NaOH(aq) + 0.98 M NaCl(aq) the corrosion of aluminum[10] occurs at 1.27 V with respect to the mercury electrode. When short circuited with a mercury surface,[10] these voltages decrease to 0.1 mV.

Under short-circuit conditions a variety of electrochemical reduction processes are favored on the mercury. Although H_2O is the most prevalent species capable of reduction in these systems, it is reduced at a very slow rate on mercury in these voltage ranges.[14] Consequently, H_2O is not directly implicated in the chemistry. On the other hand, we have shown previously[10] that dissolved O_2(aq) is rapidly reduced on mercury in the voltage range associated with the Al(W) electrode. Moreover, the peak height of the voltage curves is proportional to the concentration of dissolved oxygen. This situation appears to be quite general for oscillations that occur with little or no oxidizing species in the solution above the mercury. For these systems we present further evidence in section III that the significant chemical step occurring on the mercury is the reduction of electron acceptors from solution.

Oscillations which are triggered from near the perimeter of the mercury occur in aqueous sulfuric acid solutions containing strong oxidants such as $Cr_2O_7^{2-}$. The formation of Hg_2SO_4 proceeds spontaneously in these solutions according to

$$14H^+(aq) + Cr_2O_7^{2-}(aq) + 6Hg(l) + 3SO_4^{2-}(aq) \rightarrow 2Cr^{3+}(aq) + 3Hg_2SO_4(s) + 7H_2O(l) \qquad \mathcal{E}^\circ = +0.71 \text{ V} \quad (3)$$

Neither H^+(aq), Cr^{3+}(aq), nor H_2O is readily reduced on mercury at these voltages.[15] This leaves the Hg_2SO_4 film as the primary candidate for reduction according to the half-reaction

$$Hg_2SO_4(s) + 2e^- \rightarrow 2Hg(l) + SO_4^{2-} \quad \mathcal{E}^\circ_{red} = +0.62 \text{ V} \quad (4)$$

III. Experimental Procedures

Voltage–time curves were recorded on a Textronix 564B storage oscilloscope[10] (3A9 differential amplifier, 2B67 time base, and Polaroid camera attachment); currents were measured with a Keithley 602 electrometer; pH was measured with a Beckman Research pH meter; dissolved oxygen concentration was determined with a Beckman Fieldlab Oxygen Analyzer. A diagram of the apparatus used to study the oscillations is shown in Figure 1. The capillary geometry, in contrast to the conventional watch-glass setup, gives quantitatively reproducible results, and minimizes, if not eliminates, the purely hydrodynamic motion of the mercury. Reagent-grade chemicals were used without further purification. Carbonate-free NaOH(aq) was prepared by diluting 18 M NaOH(aq). The mercury was Ballard Bros. CP, triple-distilled grade.

Unless otherwise stated the following general procedures were used. The tungsten tip (Figure 1) was sanded to a fine point and then polished with extra fine (no. 400) sandpaper, while the tip was rotated at 1000 rpm; the tip was wiped with tissue paper. In order to obtain reproducible results it is necessary to use fresh mercury for each experiment.

A 25.0-mL sample of the appropriate aqueous solution was poured into the cup (Figure 1). The tungsten electrode tip was then positioned directly above the center of the mercury surface using a Brinkmann Model 06-20-04 micromanipulator; the precise point at which the tungsten tip touched the mercury surface was determined both visually with the aid of a beam of light shining on the surface and electrically with the oscilloscope. As soon as the oscillations were triggered by connecting the corroding aluminum wire to the W tip with a piece of copper wire, the tungsten tip was raised 0.040 mm above the mercury surface. The Al to W connection was made 2.0 min after the Al was immersed in the solution. This procedure avoids an initial transient period that follows the immersion of the Al, during which erratic results often are obtained. The voltage–time trace of the oscillation of the mercury was recorded 0.50 min after the oscillation was triggered. The Al wire exposed to the solution was 0.081 cm in diameter and 1.0 cm in length. The mercury tube diameter (i.d.) was 16.7 mm. A NaCl in agar salt bridge was used in system B (Figure 1).

The experimental procedures for the acid systems (e.g., $K_2Cr_2O_7$(aq) + H_2SO_4(aq) with a corroding iron wire connected to the tungsten tip) are similar to those described above except that the iron wire exposed to the solution was 0.005 cm in diameter and 1.0 cm in length, and the separation between the tungsten tip and the Hg surface was adjusted so the tip just touched the mercury surface at a distance of 0.12 cm from the inside of the tube.

High-speed motion picture photography was used to study the movement of the mercury surface during oscillation. The camera used was a Banz Hycam K2054E-115 16 mm. The approximate film speed employed was 1100 frames/s. The analysis of the film was carried out with the aid of a photooptical data analyzer (L. W. Van Nuys, Model 224A). This camera speed corresponds to about 100 frames per oscillation. The results of the measurements are given in Figure 2. Negative distances correspond to penetration of the mercury surface by the tungsten electrode tip; positive separations correspond to the gap between the tungsten tip and the surface.

IV. Mechanism of the Oscillations

The mercury oscillators that we have investigated can be put into two categories: those for which oscillations are triggered by placing the electrode tip near the perimeter of the mercury surface, and those which are triggered by placing the tungsten tip near the center. Off-center oscillators cannot be triggered from the center of the mercury surface, and center oscillators cannot be triggered near the side. In our experience the side-triggered oscillators always involve the formation of a visible film on the mercury surface, whereas the center-triggered oscillators do not.[10] The electrochemical mechanism of the oscillations appears to depend strongly on whether or not a film is formed. Consequently we treat these two types of systems separately.

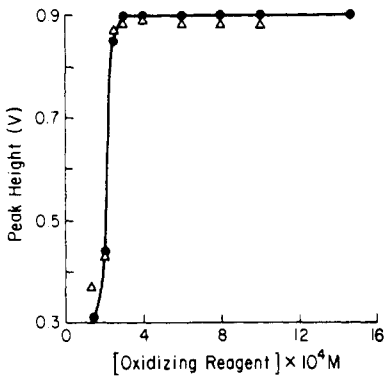

Figure 5. Dependence of peak height on the concentration of oxidizing agent for the oscillators Fe(W)|oxidizing agent (aq,M); H_2SO_4(aq,0.5 M)|Hg(l): (●) refer to $K_2Cr_2O_7$(aq) and (△) refer to $KMnO_4$(aq).

Oscillators with Film Formation. A wide variety of experiments were carried out in order to obtain clues to the mechanism of the oscillations in oscillators of the type

$$Fe(W)|H^+(aq),Cr_2O_7^{2-}(aq)|Hg(l)$$

It was found that, provided that the concentration of $Cr_2O_7^{2-}$ was within about a factor of 2 of 7×10^{-4} M, the parameters of the voltage oscillations were *not* significantly affected: (a) by the addition of Fe^{2+}(aq), Fe^{3+}(aq), Cr^{3+}(aq), or Hg^{2+}(aq); (b) by variation in the concentration of H^+(aq) over the range 0.02–2 M; (c) by a change in the nature of the strong acid used (H_2SO_4, HNO_3, HCl); (d) by bubbling O_2 or Ar through the solution; (e) by turning off the room lights; (f) by changing the temperature of the oscillator over the range 0–45 °C; (g) by a sixfold change in the height of the solution over the Hg surface; (h) by stirring the solution; (i) by the amount of Fe wire surface exposed to the solution; or (j) by substituting D^+ (D_2O) for H^+ (H_2O).

The above experimental results suggest the following conclusions regarding the mechanism of the oscillations.

(1) Hydrogen ions are not involved in or prior to the rate-determining step(s).

(2) Diffusional processes in solution are fast relative to the rate-determining step(s).

(3) Oxygen is not involved in the mechanism.

(4) The overall thermal activation energy is very small.

(5) The reduction products of $Cr_2O_7^{2-}$ and the oxidation products of Fe(s) are not involved in the rate-determining step(s).

(6) Under these conditions the electron-transfer processes are controlled solely by the voltage of the Hg surface.

The dependence of peak height on the concentration of $K_2Cr_2O_7$(aq) at $[H_2SO_4] = 0.50$ M and ionic strength 2.0 M with Na_2SO_4(aq) is shown in Figure 5. The peak height and shape are independent of $[Cr_2O_7^{2-}]$ over the range 3×10^{-4} to 15×10^{-4} M. Above 15×10^{-4} M the oscillations became irregular and at somewhat higher concentrations ceased with the formation of a thick surface film. The surface film was found by electron microprobe and X-ray powder pattern analysis to be predominantly Hg_2SO_4(s). Below about 3×10^{-4} M $Cr_2O_7^{2-}$(aq) the oscillations could no longer be triggered from the side, but they could be triggered from the center of the Hg surface. The shape of the oscillations in this region was saw-tooth rather than rectangular, and the peak height depended on $[O_2]$ and $[H^+]$. This system is discussed further under the heading "nonfilm oscillators". When $KMnO_4$(aq) or $K_2S_2O_8$(aq) is substituted for $K_2Cr_2O_7$(aq) the behavior of the oscillator is essentially the same as with $K_2Cr_2O_7$(aq). Further, using high-speed, motion-picture photography it is possible to see visual evidence of a thin surface film on the Hg. The film disappears when the Hg surface touches the W(Fe) tip.

The results described above are compatible with the production of a surface film of Hg_2SO_4 via the action of a strong oxidizing agent in the solution. However, our data are not sufficient to prove that Hg_2SO_4 is the substance comprising the film formed during the oscillations. In order to collect sufficient solid for analysis it is necessary either (a) to use a higher concentration of $Cr_2O_7^{2-}$ than the maximum for which oscillations can be obtained or (b) to apply a larger voltage (Hg^+) than that developed between the W tip and the Hg during oscillations. Furthermore, there is another substance (evidenced in the X-ray powder pattern and present at <5%) mixed in with the Hg_2SO_4. With HCl as supporting acid the solid formed is predominantly Hg_2Cl_2. With HNO_3, the solid formed (initially orange which then turns deep red) contains mercury and chromium, but its X-ray powder pattern does not correspond to any compound containing Hg and Cr that is listed in the ASTM tables. We note that HgO(s) is thermodynamically unstable

$$HgO(s) + 2H^+(aq) \rightarrow Hg^{2+}(aq) + H_2O(l) \qquad \Delta G°_{298} = -3.4 \text{ kcal}$$

under conditions where oscillations are observed. HgO is, therefore, an unlikely candidate for a surface film.

We believe that the surface film causes the oscillations in the following way. The shape of the mercury surface changes through the combined action of the W-Hg voltage difference and surface-tension changes produced by the film formation. As the Hg surface flattens electrical contact is made with the W-tip and the Hg_2SO_4 film is reduced. The *net* processes are postulated to be

film formation

$$\begin{cases} 2Hg(l) + SO_4^{2-}(aq) = Hg_2SO_4(film) + 2e^- \\ Cr_2O_7^{2-} + 14H^+(aq) + 6e^- = 2Cr^{3+}(aq) + 7H_2O \end{cases}$$

film reduction

$$\begin{cases} Hg_2SO_4(film) + 2e^- = 2Hg(l) + SO_4^{2-}(aq) \\ Fe(s) = Fe^{2+}(aq) + 2e^- \end{cases}$$

The reaction $Fe(s) + 2H^+(aq) = Fe^{2+}(aq) + H_2(g)$ occurs on the iron surface. The function of the corroding Fe wire is solely to act as an electron source (at a sufficiently negative potential) for the reduction of the Hg(l) surface film. This is evidenced by the fact that the oscillations can be driven by a power supply connected across the W and mercury electrodes in the absence of a corroding Fe wire. The reduction of the surface film involves the *net* process

$$Hg_2SO_4(film) + 2e^- = 2Hg(l) + SO_4^{2-}(aq) \qquad (5)$$

To help substantiate the proposed mechanism we carried out spectrophotometric determinations of $Cr_2O_7^{2-}$(aq) after oscillations had proceeded for 15 min. It was determined that ca. 2×10^{-8} mol of $Cr_2O_7^{2-}$ is consumed per oscillation in the plateau region of Figure 5.

Assuming that all the $Cr_2O_7^{2-}$ is consumed in oxidizing Hg to Hg_2SO_4 as our mechanism suggests, this would correspond to 1×10^{-8} mol of Hg_2SO_4/cm^2 of the Hg surface. This is in agreement with a complete monolayer coverage of the Hg surface by Hg_2SO_4 which would require 1×10^{-8} mol of Hg_2SO_4/cm^2 if the SO_4^{2-} ions are sticking out of the surface. We interpret this result to mean that in the plateau region each oscillation creates a monolayer of Hg_2SO_4 by oxidation with $Cr_2O_7^{2-}$(aq). Reduction then destroys the monolayer using electrons taken from the oxidation of Fe. The poisoning of the system at high $Cr_2O_7^{2-}$(aq) concentration may occur because the film grows too quickly to be reduced by the corroding Fe.

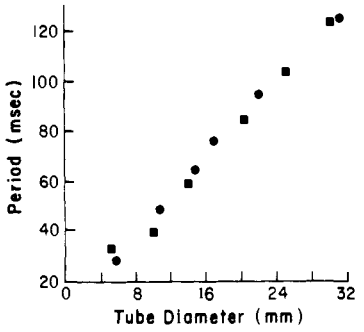

Figure 6. The period of the voltage oscillations as a function of the tube diameter. The circles are experimental points and the squares are for the limit cycle oscillations for model I for the parameter values listed in ref 27 except $D = 45$, $i_0 = 1.35 \times 10^{-3}$, $L = 0.5R^{-3}$, $Y = 80R^{-1}$ (with R = tube radius in cm).

Oscillators without Film Formation. The center-triggered oscillator that we have investigated in most detail is the system

$$\text{Al(W)}|\text{NaOH(aq)},\text{NaCl(aq)},\text{O}_2\text{(aq)}|\text{Hg(l)} \qquad (6a)$$

The experimental behavior of this system differs in several ways from the off-center oscillators described in the preceding section. We have found no evidence of the formation of a surface film in this system even when the oscillations have been followed for over 1 h. All of the center-triggered oscillators give rise to voltage oscillations with a saw-tooth shape (Figure 3a); side-triggered oscillations have a rectangular shape (Figure 3b).

With the single exception noted below, the diameter of the mercury column is the only factor that affects appreciably the period of the oscillations for any of the oscillators that we have investigated. The essentially linear dependence of the period of the oscillations on the diameter of the mercury in the tube is shown in Figure 6. It should be noted that we are not observing a phenomenon arising from the vibration of the apparatus. The oscillations can be stopped in several ways, e.g., raising the W-tip, purging the solution with argon, or adding certain reagents to the solution. Provided that the oscillations can be triggered, the *period* is not affected by temperature, solution composition, elapsed time since the onset of oscillations, solution volume, positioning of the W electrode tip, surface area of Al undergoing reaction, sharpness of the electrode tip, or stirring the solution.

The most important experimental clue to the mechanism of the oscillations in the oscillator (6) was provided by the observation that the peak height of the voltage oscillations is directly proportional to the concentration of dissolved O_2 in the solution,[10] as shown in Figure 7. By bubbling Ar through the solution the oxygen can be removed, and in the absence of O_2 the oscillations cease completely. When other reducible species, such as $Fe(CN)_6^{3-}$(aq) and Cu^{2+}(aq), are substituted for O_2, the phenomenological behavior of the resulting oscillators is essentially the same as the O_2-dependent oscillator. We have also found that oscillations can be restored in solutions which were purged of O_2(aq) by adding Br_2 or I_2. The dependence of the oscillations on concentration in these systems is qulitatively similar to that shown in Figure 7.

From measurements of the pH of the solution in contact with the Hg surface for the oscillator

$$\text{Al(W)}|\text{NaOH(aq,0.100 M)},\text{NaCl(0.90 M)}||\ \text{NaCl(aq,1.000 M)}|\text{Hg(l)} \qquad (6b)$$

we have calculated that OH^-(aq) is produced at an average rate of ca. 2×10^{-10} mol/oscillation over the period 2.0-5.0 min following the onset of the oscillations.

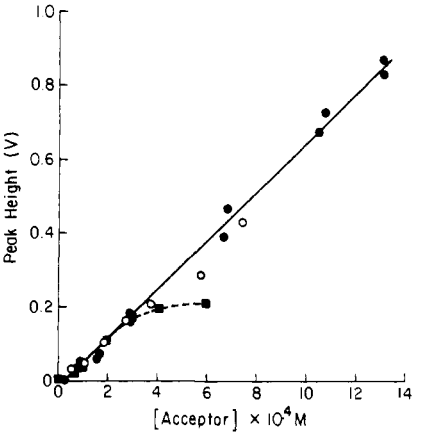

Figure 7. Dependence of peak height on the concentration of the electron acceptors: O_2(aq), $Cu(NO_3)_2$(aq), and $K_3Fe(CN)_6$(aq) in oscillators of the type Al(W)|NaOH(aq,0.040 M),NaCl(aq,0.960 M)||acceptor-(aq),NaCl(aq)|Hg(l). The ionic strength of the solution in contact with the Hg surface was maintained at 1.00 M using NaCl(aq). In all cases the period of the oscillations was constant at 75 ms. The deviation of the $K_3Fe(CN)_6$ curve from linearity was accompanied by film formation on the Hg surface. For $Cu(NO_3)_2$ the oscillations became irregular at concentrations of $Cu(NO_3)_2$ greater than about 1.25×10^{-3} M, and film formation on the surface appeared at concentrations in excess of about 8.0×10^{-4} M $Cu(NO_3)_2$(aq).

The observations noted above suggest that the *net* process[16]

$$\text{O}_2\text{(soln)} + 2\text{H}_2\text{O(l)} + 4\text{e}^- \rightarrow 4\text{OH}^-\text{(aq)} \qquad (7)$$

occurs during the short circuit of the tungsten tip and the mercury. Indeed, the average current of $2\text{-}3 \times 10^{-4}$ A/cm^2 which is observed in the voltage-interruptor experiments on this system[10] corresponds to $3\text{-}4 \times 10^{-10}$ mol of electrons per oscillation. The stoichiometry of the net reaction 7 then implies $3\text{-}4 \times 10^{-10}$ mol of OH^-/oscillation, which compares favorably with the observed value.

The source of electrons in eq 7 is the aluminum wire, which corrodes through the half-reactions

$$\text{Al(s)} + 4\text{OH}^-\text{(aq)} = \text{Al(OH)}_4^- + 3\text{e}^-$$

$$2\text{H}_2\text{O(l)} + 2\text{e}^- = \text{H}_2\text{(g)} + 2\text{OH}^-\text{(aq)} \qquad (8)$$

During short circuit the oxidation half-reaction is coupled through the tungsten to the mercury surface where adsorbed O_2 is reduced. Assuming the net process (7), about 5×10^{-11} mol of O_2 is reduced per oscillation. The rate-determining process in the reduction of O_2 does not involve H_2O, because the parameters of the voltage oscillations are unaffected by substitution of D_2O for H_2O.

The proposed reduction of O_2 *on the Hg surface* is also supported by the observation that the voltage oscillations are unaffected by the addition of the free-radical traps allyl alcohol or N_2O to the solution.

The observation that O_2(soln) is reduced during the oscillations makes it possible to interpret several other observed effects on the oscillator (6a).

(a) The peak height of the voltage oscillations is increased by stirring the solution over the mercury surface (increases the rate at which O_2(soln,bulk) can be transferred to the region near the surface).

(b) The peak height of the voltage oscillations is increased by a decrease in the height of the solution over the Hg surface (the pulsating Hg surface more effectively mixes the overlying solution).

(c) The peak height of the voltage oscillations decreases with time, Figure 8 (depletion of O_2(soln) during the oscillations).

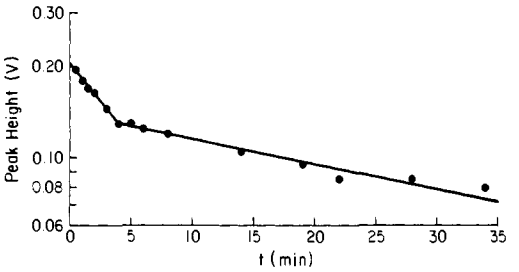

Figure 8. Semilogarithmic plot of the peak height, v_m (V), vs. the elapsed time from the onset of the oscillations for the oscillator Al(W)|NaOH(aq,0.040 M),NaCl(aq,0.960 M),O_2(aq)|Hg(l) at 25 °C. Values given are the average values for two runs.

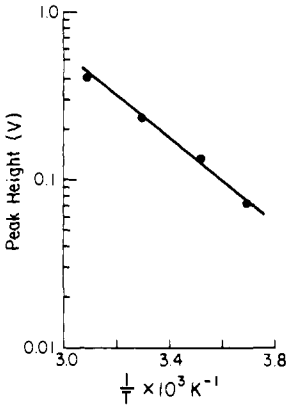

Figure 9. Dependence of the peak height of the v-t oscillations on the temperature for the oscillator Al(W)|NaOH(aq,0.040 M),NaCl(aq,0.960 M),O_2(aq,4.0 × 10^{-4} M)|NaCl(agar)|NaCl(1.000 M)|Hg(l). The temperature of the Al cup (system B, Figure 1) was held constant at 22 °C, while the temperature of the Hg cup was varied over the range 0–50 °C.

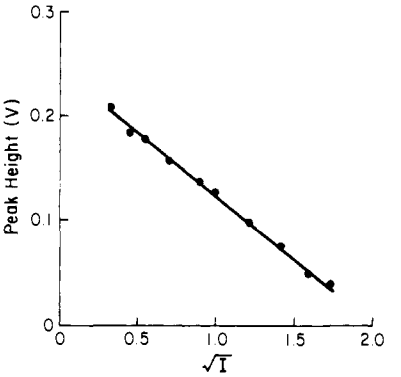

Figure 10. Dependence of peak height of the v-t oscillations on the concentration of NaOH(aq) in contact with the corroding aluminum for the oscillator: Al(W)|NaOH(aq,x M), NaCl(aq,$(1 - x)$M)|Hg(l).

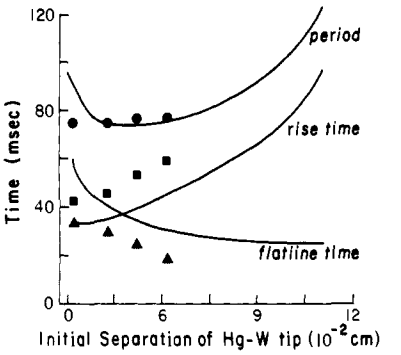

Figure 11. Characteristics of the voltage oscillation as a function of initial vertical separation of Hg and W-tip. The points are experimental values of the flat line (▲), rise time (■), and period (●) taken during the time interval 13–15 min after the onset of oscillations. The solid lines were obtained from limit cycle oscillations for model 1 as a function of $\gamma_m - \gamma_0 \equiv \Delta\gamma$. The abscissa was calculated using $\Delta s = \Delta\gamma/Y$ with Y = 140 dyn cm^{-3}; s = 0 was set at that point where smaller separations no longer produced limit cycles.

(d) The log v_m (at constant $[O_2]$) is a linear function of T^{-1} (Figure 9), $v_m = 3890 \exp(-2950/T)$, $E_a \simeq 5.8$ kcal (effect of temperature on the reaction rates and the diffusion rate of O_2(soln) and OH^-(surf)).

(e) The peak height depends on the chemical nature of both the cations and the anions in the solution and the ionic strength, Figure 10 (electrocapillary effects on mercury and ionic strength effect on the reaction rates).

The function of the corroding Al wire is solely to provide a source of electrons for the reduction of electron acceptors (e.g., O_2) on the mercury surface. This conclusion is supported by the observation that the oscillations can be driven by a power supply, provided that a sufficiently negative voltage is applied to the W electrode. The observed increase in peak height (a) with increase in the surface area of the corroding Al and (b) with increase in the concentration of OH^-(aq) in contact with the corroding Al can be ascribed to the increased stability of the Al corrosion voltage to perturbation by the mercury when the size and corrosion rates on the aluminum are increased.

The peak height, rise time, and flat-line time depend on both the vertical and horizontal position of the tungsten electrode tip. The effects of changing the vertical separation of the W-tip and the mercury surface are shown in Figure 11. Both the peak height (V) and the half-width (ms) (not shown) depend linearly upon the vertical separation of the W-tip from the Hg surface. At separations greater than about 0.65 mm voltage oscillations are not observed. The rise time plus the flat-line time is equal to the period; as the separation increases the rise time increases and approaches the period in magnitude.

Because of the curvature of the Hg surface (see Figure 4) the horizontal position of the W-tip relative to the Hg surface can be changed in two ways: (1) with the initial W to Hg separation held constant (at 0.04 mm); (2) with the depth of the W-tip in the solution held constant. In case (2) both the horizontal and vertical separations are changed simultaneously; the results for case (2) are shown in Figure 12. At fractional distances beyond about 0.66 (~5.4 mm) oscillations cannot be sustained. The results for case (1) are quite different than for case (2). As the W-tip is moved out from the center at fixed separation the peak height changes only slightly; however, at about one-third of the distance to the outside edge the period of the oscillations changes discontinuously from 75 to 43 ms. The period remains at 43 ms out to two-thirds of the distance to the outside edge; beyond this distance the oscillations cannot be sustained. This effect presumably arises from the excitation of a higher frequency shape oscillation of the Hg surface. (We have observed that in the conventional watch-glass geometry it is possible to excite at least three different shape oscillations of the mercury surface, namely, (1) a symmetric breathing mode, (2) an inverting triangular mode ("hexagonal" on inversion), and (3) an inverting cigar-shaped mode ("square" on inversion).

V. Electrocapillary Switching Mechanism

At equilibrium the shape of the mercury surface depends on the surface tension, γ. The surface tension in turn depends on the conditions and voltage of the mercury-solution interface. This is known as the electrocapillary effect.[13] When mercury is in contact with an electrolyte solution, the effect of change in voltage on γ is schematically represented in Figure 13. The maximum in the surface tension appears at the voltage

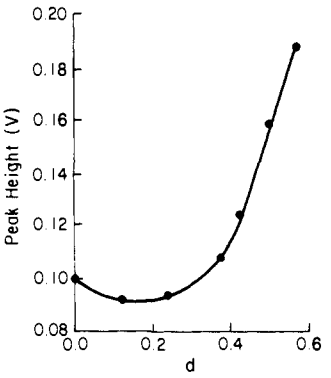

Figure 12. The effect of changing the horizontal position of the W-tip from the center of the Hg surface at fixed initial separation (0.04 mm) between the W-tip and the Hg surface. Data taken for the oxygen oscillator in eq 6b at 25 °C.

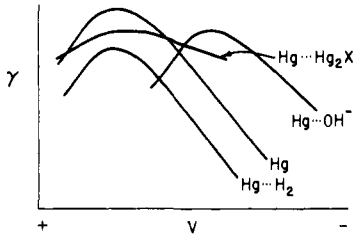

Figure 13. Schematic graphs of the surface tension as a function of voltage for mercury and for mercury with H_2, OH^-, or Hg_2X adsorbed on the surface.

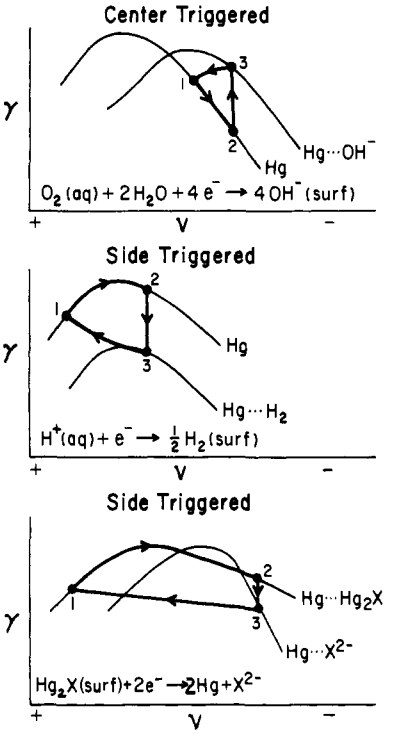

Figure 14. A representation of the cycle of surface tension changes for three different reduction processes on mercury. Step 1 → 2 represents the rapid short circuit; step 2 → 3 represents reduction occurring at the short-circuited voltage of the W-tip; step 3 → 1 occurs after short circuit is broken. See text for explanation.

at which the total electrolytic charge in the double layer is zero and is called the electrocapillary maximum. The portion of the electrocapillary curve at voltages lower than the maximum is called the "cathodic branch" and at higher voltages the "anodic branch". Because there is very little specific absorption of cations, the shape of the cathodic branch is essentially independent of the nature of the electrolyte solution.

Adsorbed ion species from the solution affect the electrocapillary curves, and on general grounds[17] it is known that they will always *lower* the surface tension at the electrocapillary maximum. If the adsorbed species are uncharged—such as H_2—this merely shifts the electrocapillary curves downward, as in Figure 13. However, for anions—such as the hydroxide anion which is released in the reduction of oxygen—the effect of increased adsorption also displaces the electrocapillary maximum to lower voltage. This is observed experimentally for a variety of anions.[18] It can be understood qualitatively, since when more anions are in the adsorbed layer a more negative voltage is required to attract the additional cations needed to achieve neutrality at the electrocapillary maximum. The effect of an Hg_2X film on the surface tension is less easily determined, although it seems likely that it would both lower and broaden the electrocapillary curve. The lowering of the surface tension for the free mercury surface is readily apparent from the flattening on a Hg drop in a watch glass when $K_2Cr_2O_7$ crystals are dissolved in acid solution covering the mercury. The broadening of the electrocapillary curve corresponds to the fact that Hg_2X is an insulator. Consequently the slope of the curve (which equals the surface charge[13]) should be smaller at a given voltage than for metallic mercury.

In our mechanism for the oscillations, the electrocapillary effect provides the switch for altering the direction of motion of the mercury. This idea can be traced back to Lippmann[8] and is clarified by an examination of our chemical mechanism along with the qualitative form of the electrocapillary curves in Figure 13. The switching mechanism depends on the way in which the mercury to electrode tip separation changes with surface tension. As discussed in section I, the flattened surface in Figure 4 occurs when the surface tension is large and the rounded surface occurs when the surface tension is small. Thus an *increasing* surface tension means an *increasing* separation for center-triggered oscillations but a *decreasing* separation for side-triggered oscillations. The opposite change in separation occurs when the surface tension decreases. To act as a switch, the surface tension must decrease the separation, s, when the mercury and the tip contact, then increase s until contact is broken, and finally decrease it again until contact is restored.

The manner in which the electrocapillary effect achieves this switching is shown for several types of oscillators in Figure 14. The path 1 to 2 represents the short-circuiting process. During short circuit there is a rapid voltage change with little chemical change on the mercury surface. When electron acceptors from solution are being reduced, this step occurs with the mercury surface relatively free of the reduced species; if an oxidant like $Cr_2O_7^{2-}(aq)$ is present in solution, the surface will be covered with Hg_2X when the short circuit begins. The step 2 to 3 corresponds to reduction on the mercury surface at the short-circuited voltage. Short circuit is broken at 3, and between 3 and 1 the voltage of the mercury increases. For the three types of oscillators shown in Figure 14, the accompanying sequence of separation changes is $\Delta s_{12} < 0$, $\Delta s_{23} > 0$, $\Delta s_{31} < 0$. This is the switching effect needed to produce the oscillations.

These considerations also provide a qualitative explanation of the switching mechanism for the "beating mercury heart" in a watch glass. In this geometry oscillations are triggered by a nail poised at the side of a mercury drop covered with acidic dichromate solution.[10] When the nail and surface are not touching, the voltage is positive and the oxidation of Hg to Hg_2X causes the surface tension to decrease, making the drop flatten. This effect continues, accelerated by the inertia of the drop, until contact between the nail and mercury occurs. Although Figure 14 shows that contact increases the surface

tension, this effect is dominated by the inertia of the drop which continues the downward motion of the mercury. The electrocapillary effect dominates the inertia only when the drop slows down. This causes the surface to readjust itself toward the equilibrium position at 3. If 3 corresponds to an arrangement in which the short circuit is broken, the surface tension continues to increase. This causes the mercury to recede from the nail until, again, the voltage is positive enough for the Hg_2X film to flatten the mercury.

VI. Kinetic Analysis

In order to help substantiate our mechanism, we have analyzed the differential equations which correspond to our mechanism for the oscillator

$$Al(W)|NaOH(aq),NaCl(aq),O_2(aq)|Hg(l)$$

When the tip is far away from the mercury, the voltage difference between the mercury and the Al(W) tip is $v = \phi_{Hg} - \phi_{Al(W)} = 1.27$ V. When the tip is placed in contact with the surface, and then slightly withdrawn, electrochemical-mechanical oscillations are observed. Evidently, the kinetically important variables are the *voltage difference, v*, the *surface concentration of hydroxide ions, c*, and the *separation between the mercury surface and the tungsten tip, s*.

The rate equations which have been proposed to describe the coupling among the variables c, v, and s are[10]

$$ds/dt = L[\gamma(c,v) - \gamma(s)] \tag{9}$$

$$dc/dt = [i_0 \exp(-v/v_0) - i_0' \exp(v/v_0')] - D(c - c_0) \tag{10}$$

$$C\, dv/dt = [i_0 \exp(-v/v_0) - i_0' \exp(v/v_0')] - \sigma(s)v \tag{11}$$

Equation 9 is based on nonequilibrium thermodynamic ideas[19] and expresses the fact that the rate of change of separation is proportional to the disequilibrium in the surface tension through the phenomenological coefficient L. Equation 10 describes the rate of change of the surface concentration of OH^- on the mercury. The first term comes from the electrochemical production and reduction of O_2 in solution and has the Butler-Volmer form.[11,12] In this equation i_0 is the cathodic current density and v_0 is 0.434 times the Tafel "b" value for the cathode reaction. The primed terms are for the reverse anodic reaction. The second term in eq 10 represents the rate of adsorption and desorption of OH^- from the adsorbed layer. The first-order rate constant for this process is D and c_0 is the surface concentration of OH^- which results from equilibrium with the bulk. For a weakly adsorbed species like OH^-, c_0 is essentially zero. The voltage equation (11) governs the change in the charge density, q, which lies on the mercury side of the double layer since $dq = C\, dv$, where C is the differential capacitance per unit area.[13] The charge density changes in the first term by electrochemical processes and in the second term by direct conduction of electrons from the aluminum. The mercury-tungsten tip conductivity is $\sigma(s)$ and is nonzero only when the tip directly contacts the mercury surface. Because of contact resistance, σ is large, but finite, when contact is made.

It should be emphasized, again, that the electrochemical processes on the aluminum do not appear in eq 9-11 except to create a short circuit when contact is made. In other words, the aluminum has been taken as a source of electrons at a fixed potential. This corresponds to the observation that the voltage of the aluminum changes only slightly if its surface area is large enough, as well as to the observation that oscillations can be triggered by an external current source whose voltage is fixed.

The electrochemical coupling in the mechanism is in eq 10 and 11 and has the standard Butler-Volmer form. Equation 9, which governs the change of the separation, depends on the electrocapillary effect and appears to be novel. Since it is eq 9 that provides the switching mechanism for the oscillations, its derivation and limitations are discussed more completely in the Appendix.

Conspicuously absent from our kinetic equations are terms explicitly involving the inertia of the mercury. Indeed, we have chosen the experimental vertical geometry in Figure 1 so as to minimize inertial effects.[10] Examination of our high-speed motion picture of the oscillations verifies that the meniscus shape changes smoothly as indicated schematically in Figure 4, and only by a small amount. Surface ripples and other elastic effects are also absent if the amplitude of the oscillations is small. On the other hand, inertial effects are crucial in the horizonal geometry of the watch glass, as mentioned in the discussion of Figure 14. For this reason our kinetic equations (9)-(11) do not apply to the watch-glass geometry.

VII. Model Equations and Solutions

Two simplified versions of eq 9-11 have been examined in detail. Both simplifications involve the electrochemical reduction of oxygen on mercury, but they differ in the rate-controlling step.

When an electron-transfer step controls the rate of reduction of oxygen, the rate terms in eq 10 and 11 are precisely the Butler-Volmer terms described there. However, since the oscillations occur at low voltages the anodic term $i_0' \exp(v/v_0')$ is negligibly small and may be ignored. Thus for reaction control the model is

$$ds/dt = L[\gamma(c,v) - (\gamma_0 + Ys)] \tag{Ia}$$

$$dc/dt = i_0 \exp(-v/v_0) - Dc \tag{Ib}$$

$$C\, dv/dt = i_0 \exp(-v/v_0) - \sigma(s)v \tag{Ic}$$

The term c_0 in eq 10 has been neglected since the equilibrium concentration of OH^- is essentially zero.[13] Also only the first two terms in a Taylor series expansion of $\gamma(s)$ (see eq 9) have been retained since the change in separation is less than 1 mm in the experiment. Thus $Y \equiv (\partial\gamma^e/\partial s)_{s=0}$ and $\gamma_0 \equiv \gamma^e(0)$.

It is possible that the slowest step in the reduction of oxygen is the rate at which oxygen diffuses to the mercury surface. In this case the reaction becomes diffusion controlled and the electrochemical rate term takes the form $i_0 - i_0' \exp(v/v_0')$. This is equivalent to setting $v_0 = \infty$ in eq 10 and 11 and leads to the second model:

$$ds/dt = L[\gamma(c,v) - (\gamma_0 + Ys)] \tag{IIa}$$

$$dc/dt = i_0 - i_0' \exp(v/v_0') - Dc \tag{IIb}$$

$$C\, dv/dt = i_0 - i_0' \exp(v/v_0') - \sigma(s)v \tag{IIc}$$

We have carried out extensive work on both of these models but will report here only the details of the work on model I. Because of a peculiarity of the coupling between the variables c, v, and s, the equations for both models can be reduced to quadrature in two distinct and easily connected regimes. This results from the fact that the short-circuited conductance, i.e., $\sigma(s)$ when $s < 0$, is very large and dominates eq Ic and IIc, whereas, when $s > 0$, contact is broken and $\sigma(s)$ vanishes. This is a switching behavior and only when contact is just being made will the term $\sigma(s)$ be dynamically important.

Shortly after contact has been made, i.e., when $s > 0$, the equations are simple to solve since then the mercury is short circuted to the tungsten and the voltage is constant. Since σ is very large at short circuit, the voltage difference is essentially zero. Substituting $v = 0$ into eq Ib and IIb leads to equations which are then easily solved. When contact is broken, solutions are also very easy to obtain since then $\sigma \equiv 0$, and eq Ic or IIc

are uncoupled from the remaining equations. The explicit solutions to these equations for $v(t)$ may be substituted into eq Ib or IIb. These equations then involve only c and the known function $v(t)$. Since these equations are first order in the time and linear in c, they can be integrated to obtain $c(t)$. Explicitly we find:

not touching ($s > 0$)

model I

$$v(t) = v_0 \ln[(i_0 t/Cv_0) + e^{v(0)/v_0}] \tag{12}$$

$$c(t) = e^{-Dt}\left[c(0)i_0 \int_0^t e^{Dt}(e^{v(0)/v_0} + i_0 t/Cv_0)^{-1}\mathrm{d}t\right] \tag{13}$$

model II

$$v(t) = v_0 \ln\left[\frac{i_0 e^{v(0)/v_0} e^{i_0 t/v_0' C}}{i_0 - i_0' e^{v(0)/v_0}(1 - e^{i_0 t/v_0' C})}\right] \tag{14}$$

$$c(t) = e^{-Dt}\left\{c(0) + i_0 \int_0^t e^{Dt}\left[\frac{i_0 e^{v(0)/v_0} e^{i_0 t/v_0' C}}{i_0 - i_0' e^{v(0)/v_0}(1 - e^{i_0 t/v_0' C})}\right]\mathrm{d}t\right\} \tag{15}$$

touching ($s < 0$)

model I

$$v(t) = v_{\text{short-circuit}} \simeq 0 \tag{16}$$

$$c(t) = (i_0/D)(1 - e^{-Dt}) + c(0)e^{-Dt} \tag{17}$$

model II

$$v(t) = v_{\text{short-circuit}} \simeq 0 \tag{18}$$

$$c(t) = [(i_0 - i_0')/D][1 - e^{-Dt}] + c(0)e^{-Dt} \tag{19}$$

In these equations $c(0)$ and $v(0)$ are the values of c and v at $t = 0$. The separation between the mercury and tungsten tip, $s(t)$, is found by solving eq Ia using the explicit solutions for $c(t)$ and $v(t)$ above. The general expression, valid for both models and for $s > 0$ or $s < 0$, is

$$s(t) = \exp(-LY\tau) \times \left[s(0) + \int_0^t e^{LY\tau}(\gamma(c(\tau),v(\tau)) - \gamma_0)\mathrm{d}t\right] \tag{20}$$

where $s(0)$ is the separation at $t = 0$.

Because of the rapidity with which the short circuit is made and broken, the solutions can be pieced together to get an accurate representation of the solutions to eq I and II. This has been done for both models and is described in section X.

It should be emphasized here that the neglect of the cathodic term in eq 10 and 11 does not affect the description of the oscillations in the calculations which follow since the oscillations occur in a voltage range in which this term is small. However, a general description of the steady states for eq 9–11 requires the inclusion of this term and its effect is discussed in section IX.

VIII. Selection of Parameters

In order to carry out calculations and compare with experiment, the electrocapillary function $\gamma(c,v)$ must be specified. This function is not accessible to the usual equilibrium measurements[13] since for fixed bulk concentrations of hydroxide, $[OH^-]$, the equilibrium surface concentration c^e is a function of the applied voltage, i.e., $c^e(v,[OH^-])$. Thus for mercury in equilibrium with a bulk solution of hydroxide the measured electrocapillary curve is $\gamma(c^e(v,[OH^-]),v)$. On the other hand, by changing the bulk concentration of hydroxide, different surface concentrations can be obtained at a fixed voltage. This gives a partial representation of the effect of the surface concentration of adsorbed hydroxide ions. Unfortunately, hydroxide is so weakly adsorbed from the bulk that these measurements do not give useful information for this experiment.[18] The general appearance of γ can be gleaned from comparable experiments[18] on strongly adsorbed anions, and this gives rise to the qualitative features represented in Figure 13. Because the oscillations occur on the cathodic branch of the electrocapillary curve, we have assumed a fixed capacitance C for the double layer and used the parabolic approximation

$$\gamma(c,v) = \gamma_m(c) - \frac{C}{2}(v - v_m(c))^2 \tag{21}$$

In eq 21 $\gamma_m(c)$ is the surface tension at the electrocapillary maximum—which is a decreasing function of the surface concentration of OH^-—and $v_m(c)$ is the voltage difference at the electrocapillary maximum—which also is a decreasing function of c. For simplicity the linear approximations

$$\gamma_m(c) = \gamma_m - ac \tag{22}$$

and

$$v_m(c) = v_m - qc \tag{23}$$

have been used. The constants v_m and γ_m are the voltage difference and surface tension at the maximum when $c = 0$. This corresponds to the equilibrium electrocapillary curves at low bulk hydroxide concentration which have been measured to be $v_m = 0.75$ V and $\gamma_m = 425$ dyn cm^{-2}. A capacitance[18] of 30 μF cm^{-2} which is typical of the cathodic branch was used. The values of a and q used were similar to those which could be estimated from Grahame's electrocapillary data.[18] The unit for surface concentrations was conveniently chosen as the number of anions cm^{-2} which corresponds to 1 μC of charge·cm^{-2}, i.e., 6.2×10^{12} ions cm^{-2}. For this "unit", a = 0.4 dyn cm^{-2}/"unit" and $q = 0.017$ V/"unit".

The diffusion constant D in eq Ib and IIb is unknown and probably voltage dependent. A simple kinetic model based on binding in a potential well[22] suggests that it has the form

$$D = \nu \exp(-\epsilon/k_B T)$$

where ν is the oscillation frequency of bound hydroxide and ϵ is a barrier height. This barrier will be increased by more positive voltages, although this effect is neglected here. An estimate of $\nu \approx 10^{13}$ s^{-1} and $\epsilon \approx 0.6$ eV gives $D \approx 50$ s^{-1}, and in the reported calculations values of D in the range 25–45 s^{-1} were used, although values as small as 10 s^{-1} and as large as 200 s^{-1} have also been used.

The equilibrium surface tension, $\gamma^e(s)$, is difficult to obtain analytically for the experimental arrangement shown in Figure 1. For a tube of small diameter, the solution to Laplace's equation is a spherical cap[23] which was used to estimate the shape of the meniscus. Since the radius of the tube in Figure 1 is the order of 1 cm, this could be used only as a guide for determining $\gamma^e(s)$ and only in the linear approximation $\gamma^e(s) = \gamma_0 + Ys$. The parameter γ_0 is the surface tension which just makes the meniscus of the mercury touch the tungsten and so depends on the *placement of the tip*. Thus γ_0 is an experimental variable and the existence of oscillations depends strongly on the size of γ_0. On the other hand, $Y = (\partial\gamma^e/\partial s)_{s=0}$ and so Y^{-1} measures how much the meniscus rises under a given change in surface tension. It depends on the radius, R, of the tube which contains the mercury, and an estimate using a spherical cap for the meniscus gives $Y \approx 500/R$ (dyn cm^{-3}). A value of $Y = 140$ dyn cm^{-3} was used in most calculations, although values between 1 and 10^4 produce oscillations, too. It should be emphasized that because of the geometry Y is positive. This should be clear from Figure 4 since an increased surface tension flattens the meniscus and so increases the separation at the center.

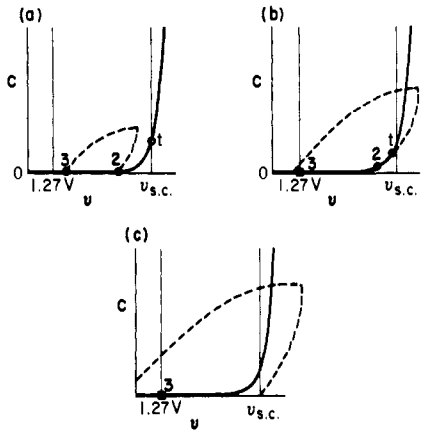

Figure 15. Schematic plots of the curves $ds/dt = 0$ (dotted line) and $dc/dt = 0$ (heavy full line) in the plane $s = 0$. The circles represent the intersection of the curves $ds/dt = dc/dt = dv/dt = 0$ and give the position of the steady states. The open circles represent a steady state with $s < 0$, the filled circles are steady states at $a \approx 0$, and the squares are steady states at $s > 0$. The curves (a)-(c) represent initial settings of the W-tip at progressively larger distances from the mercury.

The values of the Tafel parameters i_0 and v_0 for model I were taken to correspond closely to values measured experimentally for the reduction of oxygen using a periodic interrupter method.[10] The value of v_0 is fixed at $v_0 = 0.045$ V and i_0 is varied in the range 5×10^2 to 5×10^3 μC cm^{-2}. A range of values for i_0 has been used since i_0 is proportional to the bulk concentration of oxygen, which is an experimentally controlled variable. For model II, the value of v_0' was fixed at the diffusion-controlled value for a two-electron process of $v_0' = 0.052$ V. The values for i_0 and i_0' were varied in the same range as for model I.

As described in section IX the exact form of $\sigma(s)$ is irrelevant for solving eq I and II, since σ is essentially a step function with a large value for $s < 0$ and zero for $s > 0$. For use in the linear stability analysis, these values were connected by a linear function near $s = 0$ of the form

$$\sigma(s) = \sigma^* - fs \tag{24}$$

The conductance at short circuit, σ^*, has been estimated[10] to be 20 Ω^{-1}, and, if metallic contact falls to zero for a separation of $s = 10$ Å, then f is estimated to be 2×10^8 Ω^{-1} cm^{-1}.

The surface tension relaxation constant L is difficult to measure experimentally and certainly depends on the size of the tube. A value for L the order of 1 cm^3 dyn^{-1} s^{-1} was often used. This gives relaxation rates of the order of 10^2 to 6×10^3 mm min^{-1} (see Figure 2) which is in the range of experimentally measured surface relaxation rates for mercury.[24]

Values of the parameters which gave good agreement with experiment are listed in ref 27.

IX. Steady States and Linear Stability

The steady states[25] for both models are easily found using the steady-state conditions $ds/dt = dc/dt = dv/dt = 0$. For example, for model I this condition gives the simultaneous equations

$$s = (\gamma(c,v) - \gamma_0)/Y \tag{25}$$

$$c = (i_0/D) \exp(-v/v_0) \tag{26}$$

$$\sigma(s)v = (i_0) \exp(-v/v_0) \tag{27}$$

The surface on which ds/dt equals zero is defined by eq 25 and obviously has the general shape of $\gamma(c,v)$ illustrated in Figure 14; the surface on which $dc/dt = 0$ comes from eq 26 and is independent of s; eq 27 shows that the surface for $dv/dt = 0$ is independent of c. The steady states occur at the simultaneous intersection of all three surfaces.

When s is negative, σ takes the value σ^* in eq 16 and so all points on the $dv/dt = 0$ surface for $s > 0$ occur at the short-circuited voltage. This is determined from eq 27 by

$$\sigma^* v_{sc} = i_0 \exp(-v_{sc}/v_0) \tag{28}$$

The remainder of the $dv/dt = 0$ surface is very close to the $s = 0$ plane. This follows since, for s greater than a few ångstroms, σ vanishes and eq 27 has no solution. However, when $s \approx 0$, eq 24 can be substituted into eq 27 to give

$$s = [\sigma^* - (i_0/v) \exp(-v/v_0)]/f$$

which is a surface extending between $v = v_{sc}$ at $s = 0$ and $v = \infty$ at $s = \sigma^*/f \approx 10$ Å. Actually, if the voltage is high enough, the cathodic terms in eq 10 and 11 become important. This affects only the high-voltage portion of the steady-state surfaces. One effect is to cause the anodic term $i_0 \exp(-v/v_0)$ to equal the cathodic term $i_0' \exp(v/v_0')$ at the resting voltage of mercury,[10] i.e., at $v = 1.27$ V. This means that the $dv/dt = 0$ surface actually terminates for $s > 0$ at $v = 1.27$ V and that the rest of the surface is the plane $v = 1.27$ V for $s > 0$. Thus considerations of the steady states can be restricted to voltages between $v = 1.27$ V and $v = v_{sc} \approx 0$.

Because the steady states occur either close to the $s = 0$ plane or at $v = 1.27$ V or $v \approx 0$, a great deal of information about steady state can be gleaned by drawing the curves for eq 25 and 26 in the $s = 0$ plane. This is done schematically in Figure 15 for fixed chemical parameters for model I and a variety of values of γ_0. It should be recalled that a large value of γ_0 corresponds to the tungsten tip being positioned far away from the mercury and that a small value corresponds to a close positioning. Figure 15a shows that a close position leads to steady states at points 1, 2, and 3. Linear stability analysis[25] shows that in this configuration state 1 is stable while 2 and 3 are unstable. State 1 occurs below the $s = 0$ plane ("touching") at the short-circuit voltage. This corresponds to a situation in which the tungsten tip is pushed into the mercury and the short circuit is stable. When the tip is pulled back a bit, as in Figure 15b, there are still three steady states, but only 3 is stable. Thus pulling the tip away has changed the stable state 1 in Figure 15a into an unstable state. When the tip is pulled away even further, the situation in Figure 15c develops. Now only one steady state is possible at a *positive* separation and $v = 1.27$ V, the voltage of free mercury surface. This occurs when the tip is placed too far away to make contact with the mercury. It is the tip placement in Figure 15b that leads to oscillations, and the limit cycle which produces them is described in the following section.

X. Analysis of the Solutions

The solutions to the differential equations for model I are given by the quadratures in eq 12-20. These solutions are valid in the separate regimes when the mercury and tungsten tip are in contact ($s < 0$) and when contact is broken ($s > 0$). Because of the large discontinuity in the conductance at $s = 0$, these two solutions can be "pieced together" to produce an excellent approximation to the time-dependent solutions. This is a consequence of the fact that the short circuit occurs on a time scale at least four orders of magnitude faster than any of the other kinetic processes.[10] For example, if the conditions at time zero are $s(0) > 0$ with $c(0)$ and $v(0)$ arbitrary, eq 12, 13, and 20 give the values of $v(t)$, $c(t)$, and $s(t)$ *until such time* t^* *as* $s(t^*) = 0$. At this instant short circuiting begins. When the short circuiting is complete (in about 10^{-7}-10^{-6} s), the solutions in eq 16, 17, and 20 will be valid. The initial values in the $s < 0$ regime are clearly $c(0) = c(t^*)$ and $s(0) = s(t^*) = 0$ since neither of these variables changes appreciably within the short-circuiting interval. This leads to a sharp discontinuity

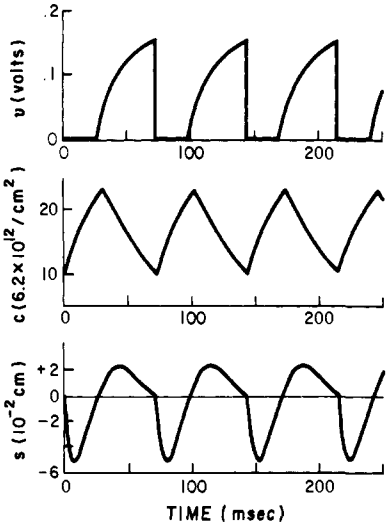

Figure 16. Voltage, concentration, and separation oscillations for the limit cycle for model I using the parameter values listed in ref 27.

in the voltage v at the instant of short circuit, but the functions c and s only have discontinuities in their slopes. The solutions in the touching region continue to be valid until a time t^{**} when $s(t^{**}) = 0$ and the short circuit is broken. Then eq 16 and 17 can be used with $v(0) = v_{sc} \approx 0$, $c(0) = c(t^{**})$, and $s(0) = s(t^{**}) \equiv 0$. When short circuit is broken all the functions are continuous, but have discontinuous slopes.

This procedure was carried out by numerically evaluating the quadratures in eq 12-20, as necessary, and the results reported here were carried out on a PDP-8 computer. The integrals in eq 12-20 were approximated using Simpson's rule. For the chosen parameter values, a time interval for the Simpson's rule calculation of 2×10^{-4} s gave three-figure accuracy in the computed values of c, v, and s. After each iteration of Simpson's rule, the value of s was tested and, if it had changed sign, say to $s < 0$, then the calculation was switched to the $s < 0$ regime.

For model I a great variety of solutions are obtained depending on the initial conditions chosen for $c(0)$, $v(0)$, and $s(0)$. Tremendous qualitative differences also occur depending on the placement of the tungsten tip above the mercury. Recall that this adjustment is accounted for by the surface tension parameter γ_0 in eq I and II, and its effect on the steady states has been illustrated in Figure 15. When the tip is adjusted close to the surface as in Figure 15b, initial conditions for voltages around the short-circuit voltage and concentrations in the range below 2.5×10^{14} ions cm^{-2} lead invariably to the limit-cycle oscillations shown in Figure 16. The motion toward the limit cycle is extremely rapid and within two oscillations the limit cycle is essentially attained. When the parameter γ_0 is adjusted so the tungsten tip is placed either far from the mercury or into the mercury no limit cycle occurs and the trajectories rapidly approach the steady states shown in Figures 15a and 15c. When the positioning of the tungsten tip is in the correct range, the limit cycle is obtained for broad ranges of the parameter values in eq I.

The behavior of the solutions of model II is qualitatively similar to those of model I and shows a limit cycle. However, no matter what values of the experimental parameters in eq II are chosen for model II, the period of the limit cycle is at least *two to three times that observed experimentally*. Furthermore, the voltage rise curves—even in the most favorable cases—become flat prior to short circuit, in contrast to the experimental curves in Figure 3a. Consequently, we have concluded that the oscillations occur under conditions of reaction control.

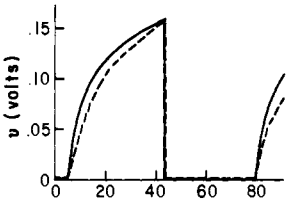

Figure 17. Comparison of experimental and theoretical voltage oscillations. The dashed line is the experimental curve shown in Figure 3a. The solid line is for the limit cycle oscillation of model I with $\gamma_0 = 403$, $Y = 400$, $i_0 = 1.1 \times 10^{-3}$, and other parameters as listed in ref 27.

XI. Comparison with Experiment

The mechanism involving reaction control gives results which agree very well with experiment. Typical results are shown in Figures 2 and 17 where the theoretical curves are compared to the experimental values of the voltage and separation. The calculated voltage corresponds closely to that measured by oscilloscope. The calculated separation between the mercury and tungsten tip has the amplitude, frequency, and general shape obtained by analyzing rapid-motion-picture photographs of the oscillations. The surface concentration of hydroxide has not been measured and the theoretical curves in Figure 16 for $c(t)$ have not been compared to experiment.

Further comparisons with experimental results have been made and are given in the figures. In these experiments a single parameter was varied and certain characteristics of the voltage oscillations were measured. In Figure 11 the experimental parameter which was varied is the initial vertical separation of the tungsten tip and the mercury surface; the resulting voltage peak height, period, flat-line time, and voltage rise time were measured. These features of the limit cycle were calculated for model I using the parameter value given in Figure 16 and varying the parameter γ_0. According to eq 17 $\Delta\gamma_0/Y$ corresponds to a change in the positioning of the tip distance, and the theoretical results are plotted in Figure 11 as a function of this distance. The remarkable experimental result that the period is independent of the position of the tip is nicely reproduced by the calculation over a large range of separations. Similarly the linear increase of the voltage rise time and decrease of the duration of the short circuit as the tip is pulled away are found.

In Figure 6 the effect of the change of radius of the tube containing the mercury on the oscillation period is shown. The period is seen to increase linearly with diameter. This is compared to the effect of changing the parameters Y and L in model I. This comparison is made since treating the mercury meniscus as a spherical cap implies $Y \propto R^{-1}$. Also the discussion in the Appendix suggests that L depends on the mass of the mercury in the meniscus and, probably, $L \propto R^{-3}$. For purpose of this calculation $Y = 80R^{-1}$ cm^4 dyn^{-1} and $L = 0.5R^{-3}$ cm^6 dyn^{-1} s^{-1}. Figure 6 shows that the period of the limit cycle is a reasonably linear function of R and in good agreement with experiment.

Finally Figure 18 gives the experimental results for the voltage peak height when the oxygen concentration is varied in the solution over the mercury by a factor of 2. For the data represented the period is 75 ms and the peak height is a linear function of the oxygen concentration. For model I the anodic current density i_0 is proportional to the oxygen concentration, so the experiment corresponds to doubling i_0. The calculated results for model I are also given in Figure 18 and, again, agreement with the experiment is reasonable.

Model I agrees with a number of qualitative experiments, too. For example, when the tungsten tip is moved to the side of the meniscus, oscillations do not occur. From the geometry

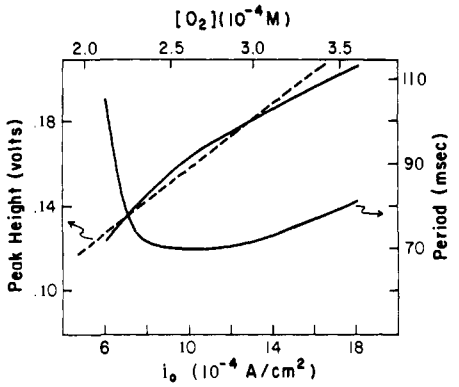

Figure 18. Peak height of voltage oscillations as a function of dissolved oxygen. The dashed line comes from the experimental in Figure 7; the solid lines were obtained from the limit cycle oscillations for model I using the parameters listed in ref 27. The experimental period for the data shown is 75 ± 2 ms.

of Figure 4 it can be seen that at the side of the meniscus an *increase* in surface tension *decreases* the separation. Thus the parameter $Y = \partial\gamma^e/\partial s$ is *negative* in this arrangement. As a consequence eq 25 shows that the surface $ds/dt = 0$ is inverted when the tungsten tip is moved to the side of the meniscus. Drawing diagrams like those in Figure 15, one easily finds that there are stable steady states which prevent a limit cycle from developing. These occur at the short-circuit voltage for close contact and at the free mercury voltage when the tip is placed far away.

The quality of the agreement between experiment and the calculations convinces us that the mechanism summarized by eq 9-11 suffices to explain the oscillations in this mercury-heart-like system.

Acknowledgments. The financial support of this research by NATO Research Grant 696, the UCD Committee on Research, and NSF Grant CHE 77-01542 is gratefully acknowledged. We also thank Richard Kulmann for the high-speed photography, Daniel Scherson for the collection of data from the films, James Tilden and James Schwellenbach for computer programming assistance, and Herbert Stenschke for helpful discussions on mechanisms of the oscillations.

Appendix

In the geometry of Figure 4, three surfaces change if the surface tension causes the mercury-solution interface to change. For example, if the surface flattens the mercury-solution interfacial area A_1 decreases, the solution-glass area A_2 decreases, and the mercury-glass area A_3 increases. On the other hand, if the surface forces produce a hydrodynamic motion (capillary waves[26]) on the mercury, these ripples may affect only the size of the mercury-solution interface. Under a wide range of experimental conditions, high-speed motion-picture photography has shown that the surface areas change shape in the smooth fashion indicated by Figure 4 and that ripples in the surface are absent. This means that velocity gradients and purely inertial effects in the mercury can be neglected. The only remaining causes for shape changes, then, are purely dissipative processes.

According to the linear theory of irreversible thermodynamics, a change in a state variable is caused by a deviation in the intensive variables from their equilibrium values.[19] Since velocity gradients are unimportant, the state variables for a system which includes the surface region are the three areas A_1, A_2, and A_3 and the masses of the mercury, m_{Hg}, and water, m_{H_2O}, in this region. The corresponding intensive variables are the three surface tensions γ_1, γ_2, and γ_3 and the chemical potentials μ_{Hg} and μ_{H_2O}. If the surface is in a condition of nonequilibrium, the surface tensions have nonequilibrium values. Furthermore the nonequilibrium arrangement can lead to nonequilibrium chemical potentials if the masses of mercury and water in the surface region are displaced to nonequilibrium heights. The deviations in these quantities from their equilibrium values are the thermodynamic "forces".

The flux-force relationships for the effect of surface tension should be

$$dA_i/dt = \sum_{j=1}^{3} K_{ij}(\gamma_j - \gamma^e_j) + k_{i\mathrm{Hg}}(\mu_{\mathrm{Hg}} - \mu^e_{\mathrm{Hg}}) + k_{i\mathrm{H_2O}}(\mu_{\mathrm{H_2O}} - \mu^e_{\mathrm{H_2O}})$$

$$dm_{\mathrm{H_2O}}/dt = \sum_{j=1}^{3} K_{\mathrm{H_2O},j}(\gamma_j - \gamma^e_j) + k_{\mathrm{H_2O,Hg}}(\mu_{\mathrm{Hg}} - \mu^e_{\mathrm{Hg}}) + k_{\mathrm{H_2O,H_2O}}(\mu_{\mathrm{H_2O}} - \mu^e_{\mathrm{H_2O}})$$

$$dm_{\mathrm{Hg}}/dt = \sum_{j=1}^{3} K_{\mathrm{Hg},j}(\gamma_j - \gamma^e_j) + k_{\mathrm{Hg,Hg}}(\mu_{\mathrm{Hg}} - \mu^e_{\mathrm{Hg}}) + k_{\mathrm{Hg,H_2O}}(\mu_{\mathrm{H_2O}} - \mu^e_{\mathrm{H_2O}}) \quad \text{(A-1)}$$

The matrix of coefficients K_{ij} and k_{mn} represents linear responses of the area and masses to disequilibrium in the surface tension and height of the center of masses. The relationships in eq A-1 apply no matter where the boundaries of the system are taken. Convenient boundaries are the sides, top, and bottom of the tube in Figure 4. This means that the masses of water and mercury are fixed and eliminates the last two equations since $dm_{Hg}/dt = dm_{H_2O}/dt = 0$. Furthermore the fixed area at the side of the tube implies that $dA_2/dt = -dA_3/dt$. These three conditions can be used to eliminate the chemical potentials and γ_3 from eq A-1 to obtain

$$dA_1/dt = L_{11}\Delta\gamma_1 + L_{12}\Delta\gamma_2$$
$$dA_2/dt = L_{21}\Delta\gamma_1 + L_{22}\Delta\gamma_2 \quad \text{(A-2)}$$

where the coefficients L_{ij} are algebraic combinations of the K's and the k's in eq A-1 and $\Delta\gamma_i \equiv (\gamma_i - \gamma^e_i)$. These equations simplify further because under the experimental conditions the glass-solution surface tension is not perturbed from equilibrium. Thus $\gamma_2 - \gamma^e_2 \equiv 0$ and so

$$dA_1/dt = L_{11}\Delta\gamma_1 \quad \text{(A-3)}$$

Since the area A_1 is a smooth function of the height of the meniscus, $ds = B\,dA_1$ and consequently

$$ds/dt = L(\gamma - \gamma^e)$$

where L is BL_{11}.

References and Notes

(1) Chemistry Department, California State University, San Diego, Calif.
(2) Hedges, E. S.; Meyers, J. E. "The Problem of Physico-Chemical Periodicity", Arnold: London, 1926.
(3) Bonhoeffer, K. F. *J. Gen. Physiol.* **1948**, *32*, 69-91.
(4) Nicolis, G.; Portnow, J. *Chem. Rev.* **1973**, *73*, 365-384.
(5) Wojtowicz, J. "Modern Aspects of Electrochemistry", Vol. 8; Bockris, J. O'M., Conway, B. E., Eds.; Plenum Press: New York, 1973; pp 47-120.
(6) Noyes, R. M.; Field, R. J. *Annu. Rev. Phys. Chem.* **1975**, *25*, 95-119.
(7) Keizer, J. *J. Chem. Phys.* **1976**, *64*, 1679-1687, 4466-4474.
(8) Lippmann, G. *Ann. Phys. (Leipzig)* **1873**, *149*, 565-561.
(9) Hoff, H. E.; Geddes, L. A.; Valentinuzzi, M. E.; Powell, T. *Cardiovasc. Res. Cent. Bull. (Houston)* **1971**, *9*, 117-130.
(10) Lin, S.-W.; Keizer, J.; Rock, P. A.; Stenschke, H. *Proc. Natl. Acad. Sci. U.S.A.* **1974**, *71*, 4477-4481.
(11) Vetter, K. J. "Electrochemical Kinetics", Academic Press: New York, 1967; Chapter 2.
(12) Erdey-Grúz, T. "Electrochemical Kinetics", Academic Press: New York, 1972; Chapters 1 and 2.
(13) Grahame, D. *Chem. Rev.* **1947**, *41*, 441-500.
(14) Akopyan, A. U. *Russ. J. Phys. Chem. (Engl. Transl.)* **1959**, *33*, 82.
(15) Reference 12, Chapter 4. Randles, J. E. B.; Somerton, K. W. *Trans. Faraday Soc.* **1952**, *48*, 937-942.
(16) Reference 12, pp 223-239.
(17) Frenkel, J. "Kinetic Theory of Liquids", Dover Publications: New York, 1955; pp 316-318.
(18) Reference 13, Table I, p 451, and Figures 7 and 8, p 464.
(19) De Groot, S. R.; Mazur, P. "Non-Equilibrium Thermodynamics", North-

Holland Publishing Co.: Amsterdam, 1961; Chapter IV.
(20) Mohilner, D. "Electroanalytical Chemistry", Vol. 1; Marcel Dekker: New York, 1966; pp 377–391.
(21) Bockris, J. O'M.; Reddy, A. K. N. "Modern Electrochemistry", Vol. 2; Plenum Press: New York, 1973; pp 1072–1074.
(22) Mott, N. F.; Watts-Tobin, R. J. *Electrochim. Acta* **1961**, *4*, 79, section 8.
(23) Moore, W. "Physical Chemistry", 4th ed.; Prentice-Hall: Englewood Cliffs, N.J.; p 479.
(24) Wilkinson, M. C. *Chem. Rev.* **1972**, *72*, 575, section VIIB.
(25) Minorsky, N. "Non-Linear Oscillations", Van Nostrand: Princeton, N.J., 1962.
(26) Landau, L. D.; Lifshitz, E. M. "Fluid Mechanics", Pergamon Press: Oxford, 1959; Chapter VII.
(27) Parameter values which produce limit cycle oscillations for model I: v_0 = 0.045 V, D = 25 s^{-1}, Y = 300 dyn cm^{-3}, γ_0 = 395 dyn cm^{-2}, C = 30 μF cm^{-2}, v_m = 0.75 V, q = 0.017 V/"unit", a = 0.4 dyn·cm^{-2}/"unit", i_0 = 9 × 10^{-4} A cm^{-2}, L = 1 cm^3 dyn^{-1} s^{-1}, γ_m = 425 dyn cm^{-2}, "unit" = 6.2 × 10^{12} ions cm^{-2}.

Reactions of Methyl Cations with Ethylsilanes[1]

G. W. Goodloe and F. W. Lampe*

Contribution from the Davey Laboratory, The Pennsylvania State University, University Park, Pennsylvania 16802. *Received March 7, 1979*

Abstract: The gas-phase reactions of CH_3^+ with $(C_2H_5)_nSiH_{4-n}$ (n = 1, 2, 3, 4) have been studied in a tandem mass spectrometric apparatus. Reaction cross sections at 1 eV kinetic energy in the laboratory system have been determined by direct comparison with the known cross section for hydride ion transfer from SiH_4 to CH_3^+. The major reactions are charge transfer, hydride ion transfer, and ethide ion ($C_2H_5^-$) transfer from the silane to CH_3^+. A rather surprising result is that, except for the case of $C_2H_5SiH_3$, ethide ion transfer is the predominant process. Isotopic labeling of the reactant ions shows only minor (<10%) incorporation of the label into the ionic products which is interpreted to mean that the major part of the reactions are either direct processes or proceed through complexes that do not involve pentavalent silicon.

Introduction

Recently[2] we reported the results of a study of the gas-phase reaction of CH_3^+ ions with the methylsilanes, $(CH_3)_nSiH_{4-n}$, when n = 1, 2, 3, 4. A very surprising feature of these results was the always important and sometimes dominant contribution to the total reaction by methide ion (CH_3^-) transfer from the silane to the attacking CH_3^+ ion. The cross sections for the methide ion transfer are comparable to those of the expected hydride ion transfer process in the case of $(CH_3)_2SiH_2$ and are larger than those for hydride ion transfer when $(CH_3)_3SiH$ and $(CH_3)_4Si$ are the targets of the reactant CH_3^+ ions. In order to investigate whether this unexpected alkyl anion abstraction from alkylsilanes might be a general reaction and not one limited to the methylsilanes, we have studied the reactions of gaseous CH_3^+ ions with the ethylsilanes, $(C_2H_5)_nSiH_{4-n}$, when n = 1, 2, 3, 4. This paper is a report of our findings.

Experimental Section

1. Apparatus and Techniques. The experiments were carried out in an ion-beam-target gas apparatus that has been described previously.[2] Briefly it consists of a modified plasma ion source (Colutron Corp.) for ion formation, a Wien velocity filter for reactant-ion selection, a collision chamber for reaction of the mass-selected ions with the target molecules, and a quadrupole mass filter for analysis of the ionic products. Electrostatic lenses are used to focus the ion beam into the Wien filter, to decelerate the reactant ions to energies in the range of 0.5-5 eV before they enter the collision chamber, and to focus the ionic products into the quadrupole mass filter for analysis.

We have examined further the question of internal energy in the CH_3^+ ions produced in the plasma source by measurement of the energy threshold for the known[2-4] endothermic reaction

$$CH_3^+ + (CH_3)_3SiH \rightarrow CH_3SiH^+ + CH_4 + C_2H_5 \qquad (1)$$

On the basis of available thermochemical data[3,4] the standard enthalpy change of (1) is ΔH° = 1.5 ± 0.3 eV. We find experimentally a threshold energy of 1.6 ± 0.2 eV in the center-of-mass system which is in excellent agreement with the thermochemical values for the endothermicity. This agreement strongly suggests that internal excitation energy in the CH_3^+ ions is at most 0.4 eV and is probably smaller.

Absolute cross sections for the reactions of CH_3^+ ions with the various ethylsilanes were determined at 1 eV laboratory energy by direct comparison with the process[5,6]

$$CH_3^+ + SiH_4 \rightarrow CH_4 + SiH_3^+ \qquad (2)$$

the cross section of which we have redetermined to be σ_2 (1 eV, lab) = 54 ± 2 Å^2. The measured cross sections were extrapolated to the limit of zero pressure in the collision chamber in order to eliminate the influence of further reactions of product ions. Pressures in the collision chamber were measured with a capacitance monometer and were varied from 0.5 to 2.0 × 10^{-3} Torr. We believe that the cross sections measured at 1 eV laboratory energy of CH_3^+ are accurate to within ±15%.

The form of dependence of relative cross section, i.e.

$$\sigma_{rel} = i_{product}/i_{CH_3^+}P$$

where the i's are currents and P is the pressure, on the kinetic energy of CH_3^+ was used to classify the reactions as exothermic or endothermic. The cross sections of endothermic reactions increase from zero at the energy threshold to a broad maximum, while the cross sections for exothermic processes usually decrease monotonically with increasing energy. All ion intensities were corrected for the naturally occurring isotopes of silicon and carbon, namely, ^{29}Si = 4.7%, ^{30}Si = 3.1%, and ^{13}C = 1.1%.

2. Materials. SiH_4 was purchased from the Matheson Co. while $(C_2H_5)_2SiH_2$, $(C_2H_5)_3SiH$, and $(C_2H_5)_4Si$ were purchased from Penninsular Chemresearch. $C_2H_5SiH_3$ was prepared by the reduction of $C_2H_5SiCl_3$ (Peninsular Chemresearch) with $LiAlH_4$ (Alfa Inorganics). CH_4, CD_3H, and $^{13}CH_4$, which were used in the ion source to produce the CH_3^+, CD_3^+, and $^{13}CH_3^+$ reactant ions, were obtained from Phillips Petroleum Co., Merck Sharp and Dohme, and Stohler Isotopes, respectively. All gases and liquids were subjected to freeze-pump-thaw cycles on a high-vacuum line prior to use.

Results and Discussion

1. Exothermic Reactions. The reactions of CH_3^+ ions with ethylsilanes are somewhat more complex but similar to the reactions of CH_3^+ with the methylsilanes.[2] Thus for $C_2H_5SiH_3$, $(C_2H_5)_2SiH_2$, and $(C_2H_5)_3SiH$, we find as major reactions (1) hydride ion transfer from the silane to the CH_3^+ ion; (2) ethide ion transfer from the silane to the CH_3^+ ion; (3) a more complex process in which the attacking CH_3^+ moiety is incorporated into the ionic product. As in the case of

0002-7863/79/1501-5649$01.00/0